Stem Cell Research (2013) 11, 1365–1377

Available online at www.sciencedirect.com

ScienceDirect

www.elsevier.com/locate/scr

Onset of heterogeneity in culture-expanded bone marrow stromal cells

Matthew J. Whitfield[a], Wong Cheng J. Lee[b], Krystyn J. Van Vliet[a,b,c,*]

[a] Department of Materials Science and Engineering, Massachusetts Institute of Technology, Cambridge, MA 02139, USA
[b] BioSystems and Micromechanics (BioSyM) IRG, Singapore–MIT Alliance for Research and Technology (SMART) Centre, Singapore
[c] Department of Biological Engineering, Massachusetts Institute of Technology, Cambridge, MA 02139, USA

Received 14 May 2013; received in revised form 10 September 2013; accepted 11 September 2013
Available online 21 September 2013

Abstract Inconsistencies among in vitro and in vivo experiments using adult mesenchymal stem cells (MSCs) confound development of therapeutic, regenerative medicine applications, and in vitro expansion is typically required to achieve sufficient cell numbers for basic research or clinical trials. Though heterogeneity in both morphology and differentiation capacity of culture-expanded cells is noted, sources and consequences are not well understood. Here, we endeavored to observe the onset of population heterogeneity by conducting long-term continuous in vitro observation of human adult bone marrow stromal cell (BMSC) populations, a subset of which has been shown to be stem cells (also known as bone marrow-derived MSCs). Semi-automated identification and tracking of cell division and migration enabled construction of cell lineage maps that incorporated cell morphology. We found that all BMSCs steadily grew larger over time; this growth was interrupted only when a cell divided, producing two equally sized, morphologically similar daughter cells. However, a finite probability existed that one or both of these daughters then continued to increase in size without dividing, apparently exiting the cell cycle. Thus, larger BMSCs are those cells that have exited the normal cell cycle. These results hold important implications for MSC in vitro culture expansion and biophysical sorting strategies.

Introduction

Adult human mesenchymal stem cells (MSCs) are multipotent cells that have been isolated from various tissues and differentiated in vitro into multiple mesodermal lineages such as osteoblasts, adipocytes, and chondrocytes (Caplan, 1991). These cells offer certain practical advantages over embryonic stem cells for therapeutic use, as adult human MSCs can be self-donated (Hare et al., 2012), have exhibited lower risk of teratomas (Knoepfler, 2009), and are not subject to the same ethical issues (Zomorodian and Baghaban Eslaminejad, 2012). Bone marrow stromal cells (BMSCs), a subset of which has been shown to be stem cells (also known as bone marrow-derived mesenchymal stem cells) are currently in clinical trials for graft versus host disease (GVHD), and are widely studied for both tissue repair and immune therapies. However, BMSC-based therapies in humans have produced inconsistent results that have been attributed to donor-to-donor variability (Siddappa et al., 2007), differing isolation/culturing protocols (Seeger et al., 2007), and functional heterogeneity within primary cell cultures or clonal populations of bone marrow-derived MSCs (Muraglia et al., 2000).

Abbreviations: MSC, mesenchymal stem cell; BMSC, bone marrow stromal cell; GVHD, graft versus host disease.

* Corresponding author. Van Vliet Group, 8-237, 77 Massachusetts Ave., Cambridge, MA 02139.; Phone: +1 617 253 3315.
E-mail address: krystyn@mit.edu (K.J. Van Vliet).

1873-5061/$ - see front matter © 2013 Elsevier B.V. All rights reserved.
http://dx.doi.org/10.1016/j.scr.2013.09.004

The inability to isolate pure populations of MSCs for therapeutic applications has largely stemmed from the lack of effective and reproducible methods to isolate MSCs; these cells do not express sufficiently specific biomolecular surface markers (Halfon et al., 2010; Pevsner-Fischer et al., 2011; Oswald et al., 2004). Conventional procedures for isolating MSCs for research and clinical applications frequently rely on in vitro selection of plastic-adherent mononuclear cells from the bone marrow. While prospective isolation of bone marrow-derived MSCs based on the minimal criteria for defining human MSCs proposed by the International Society for Cellular Therapy (Dominici et al., 2006) has helped minimize differences among laboratories, the list of proposed biomolecular markers alone does not strictly characterize MSCs (Bianco et al., 2008). Therefore, researchers have relied on in vitro potency assays to evaluate and identify MSCs; the inadequacies of such approach are that it is both retrospective and does not reliably predict cell functions in vivo. For example, it has been reported that in vitro osteogenic differentiation assays may not reflect the ability of MSCs to form heterotopic osseous tissues in vivo (Kuznetsov et al., 1997). Additionally, a recent study on GVHD patients administered with MSCs revealed no correlation between the ability of the MSCs to suppress T cell proliferation in vitro and clinical efficacy in vivo (von Bahr et al., 2012).

Another approach to identify MSCs is quantitative comparison of physical or mechanical characteristics of the cells (Maloney et al., 2010; Darling et al., 2008). Specifically, different morphologies have been used to describe MSCs cultured in vitro. MSCs have been described as fibroblastoid cells (Kuznetsov et al., 1997), spindle shaped cells (Xu et al., 2004), and a combination of very small round cells and flattened enlarged cells (Colter et al., 2001). The smaller cells are typically considered as more "naive" and capable of tri-lineage differentiation, while the larger cells have been reported to be more mature and restricted in differentiation potential (Colter et al., 2001). It has been observed in clonal cultures of BMSCs that smaller cells tend to reside at the periphery while the larger cells are more prevalent in the colony center (Ylostalo et al., 2008). Several studies have explored the source of this morphological and functional heterogeneity, and attributed this variously to: (1) reprogramming upon removal from the in vivo marrow niche (Zipori, 2010); (2) increased mutation probability due to high oxygen tension under in vitro culture conditions (Wagner et al., 2010); (3) stochastic or deterministic changes in the rate of replicative senescence (Wagner et al., 2010); (4) differences in commitment and maturation within the population (Ratajczak et al., 2008); (5) cell cycle stage (Lee et al., 2011); and (6) variation in culture conditions among many cells in a single tissue-culture dish (Bruder et al., 1997). Some studies point to cell plating density or cell–cell contact as the main contributor to changes in cell size and morphology (Ylostalo et al., 2008; Colter et al., 2000). However, other reports have demonstrated that cell density has no significant effect on MSC phenotype (Haack-Sørensen et al., 2012) and that small cells have been observed to arise in cultures that started with only large cells, and vice versa (Neuhuber et al., 2008). Therefore it is, to date, unclear how putative MSCs that exhibit different sizes and morphologies within BMSC cultures are related and may differ functionally.

Although it is anecdotally established that the size of attached BMSCs increases over time and that more of these larger cells are observed with increasing passage number, past observations are based on static observations of culture or are population based over time. Several questions have not been fully answered: How do the differences in cell size arise? Does the original cell population include subpopulations that change in proportion over time? Can smaller cells become larger cells, and vice versa? Do BMSCs divide asymmetrically to make some daughter cells larger than others? Do small cells stay small upon division, to maintain a distinct subpopulation, but then proliferate faster to the point of senescence and disappearance from the culture at early passages (Colter et al., 2001)?

An approach that has shown promise for answering these types of questions in other stem cell systems, and is becoming increasingly feasible with advanced computing power and improved tracking algorithms, is long-term in vitro imaging of individual stem and progenitor cells (Schroeder, 2011). Long-term imaging can enable the construction of cell lineage maps, tracking the progression from parent cell to daughter cells and revealing the emergence of properties of interest. For example, long-term imaging has provided data to detail the complex commitment hierarchy of embryonic (Ravin et al., 2008) and adult (Costa et al., 2011) neural stem cells, successfully captured instances of hemogenic endothelial cells giving rise to blood cells (Eilken et al., 2009), and allowed the comparison of cell cycle time, migration speed, and growth kinetics between hematopoietic stem cell siblings (Scherf et al., 2012). Here, we utilize long-term in vitro imaging to address some of the outstanding questions regarding cell-size heterogeneity in commercially purified, culture-expanded BMSCs.

We demonstrate changes in size (suspended cell diameter and adherent cell spread area) of adult human BMSCs across in vitro passages. We then quantify the onset of heterogeneity in cell size and division rate among BMSCs during extended timelapse imaging in vitro within a single passage. We construct cell lineage trees showing both the timing of cell division and cell size over time for descendants from an initial population of cells. We can thus ascribe a generational "age" to individual cells based upon the number of cell divisions since the start of the observations, so that "younger" generation cells have undergone fewer previous divisions than their "older" counterparts. Additionally, we calculate cell "lifetime" as the time from when cell A first splits (from its sister cell B to complete the mitotic event) to when cell A begins to divide itself (giving rise to its own pair of daughter cells). We find that large cells are not necessarily either younger or older cells than their smaller counterparts, but rather are cells from any generation that have stopped dividing. These findings quantify and identify the source of size-based heterogeneity within in vitro BMSC populations, which can enable culture standardization and may allow for more effective purification of bone marrow-derived mesenchymal stem cells.

Materials and methods

Cell culture

Cells from multiple commercial sources were used. We refer to these cells as human bone marrow stromal cells (BMSCs), though

we note that these initial populations are also referred to in the literature and commercially as adult human, bone marrow-derived MSCs. BMSCs used for long-term imaging were purchased from ReachBio, and received at passage 1 (p1). Cells were seeded at ~2000 cells/cm^2 on tissue culture-treated polystyrene (BD Falcon) flasks and passaged with 0.05% trypsin–EDTA (Gibco) every 7–8 days after about two population doublings through p4. The MSC population had thus undergone approximately 8 doublings before long-term imaging began. Cells were grown in an incubator maintained at 37 °C and 5% CO_2 with a complete medium (StemCell Technologies MesenCult MSC basal medium and MSC stimulatory supplement) exchange every 3–4 days. In a repeat long-term imaging experiment, the results of which are shown in the Supplementary document, BMSCs purchased from Lonza were cultured at ~500 cells/cm^2 and passaged through p3 for a total of ~12 population doublings. All other media and conditions were identical for this repeat experiment.

Image acquisition

For long-term imaging, cells were seeded in the complete media described above, at 500 cells/cm^2 on a glass bottomed 60 mm-diameter Petri dish; the glass was coated with 50 μM human plasma fibronectin (Sigma) to improve cell attachment as described previously (Treiser et al., 2010). This dish was placed on an inverted microscope (Olympus IX51, Olympus Inc., USA) with an automatic stage (ProScan II, Prior Scientific) and enclosure (WeatherStation, Precision Control) to maintain 37 °C and 5% CO_2 during imaging. Phase contrast images were acquired every 10 min at 10× for 138 h (5.75 days), starting 2 h after seeding. A 5 × 5 grid of images was acquired at two different locations within the same plate producing two 4.3 × 3.3 mm fields of view. Imaging and stage movement were controlled through MetaMorph (Molecular Devices), and the cell medium was exchanged once midway through the imaging experiment (day 3).

Image analysis and cell tracking

Using both Matlab (MathWorks, Natick, MA) and CellProfiler (Carpenter et al., 2006), individual images were corrected for illumination, background flattened and montaged, followed by a second background flattening and background subtraction on the montaged image. This resulted in cells visible against a black background, but did not segregate touching cells. No sufficiently accurate algorithm was identified to automatically separate cells that shared a border. Therefore, contacting cells were separated manually by drawing a line of 5 pixel (6.45 μm) width between cells (see Supplemental for further discussion of manual processing). Artifacts such as cellular debris were also removed at this step. Cells were identified at each time point and tracked over time using a CellProfiler algorithm based on cell overlap with the previous image. Although a complete set of images was acquired every 10 min, it was found that accurate cell tracking could be accomplished by analyzing every third image (30 min between sequential images). Finally, Matlab scripts were written to analyze and display the results. In total, 1336 cells were tracked for at least some time period over the course of the imaging experiment. Depending on the metric being assessed, different subsets of these cells were analyzed. For instance, cells that entered the field of view from the periphery were tracked and considered when analyzing cell–cell contacts; however, because prior history was unknown, these cells were excluded from all other analyses. Supplementary Table S1 indicates which subsets were used for each of the results detailed below.

Senescence-associated ß-galactosidase staining

Senescence was quantified via staining for β-galactosidase (Cell Signaling Technology, Danvers, MA), according to manufacturer's instructions. Briefly, BMSCs at passage 5 were seeded in replicates of four wells at 500 cells/cm^2 and grown for seven days. Wells were rinsed twice with DPBS containing Ca^{2+} and Mg^{2+}, then fixed with 4% paraformaldehyde, stained, and imaged under bright field (Olympus IX81, Olympus Inc., USA).

Statistical analysis

Non-parametric statistical analyses were conducted via Matlab to test for statistically significant differences among groups, as cell size, cell lifetime, and cell contact related data failed tests for normality (Jarque–Bera test). The Kruskal–Wallis one-way analysis of variance was used to determine if any significant differences existed among groups at the $p < 0.05$ level. If so, protected Wilcoxon rank sum (Mann–Whitney U) tests were conducted to identify which groups were significantly different at the $p < 0.05$ level unless otherwise stated. For boxplots, box edges are the 25th and 75th percentiles, the middle line is the median, the notch around the median represents the 95% confidence interval, and points outside the whiskers are outliers (exceeding 1.5 times the length of the box away from the box edges).

Model of in vitro cell expansion

A simple stochastic computational model was developed to investigate how our cell-tracking observations within a single passage would extrapolate to observations of cell population changes over time (multiple passages) in culture. From a small starting population, Matlab was used to simulate the replication, senescence, and size growth of individual cells over the time period of several passages. See Supplemental for complete model description.

Results

Static observations of changing cell size across passages

We and others have observed anecdotally that the average size of human adult BMSCs increases over successive passages in culture, for both adherent cells and suspended cells after trypsinization between each passage (Fig. 1). At low passages, most adherent BMSCs are small, spindle shaped with few large, round cells. Over increased passages, however, Fig. 1 illustrates that the proportion and

size of these larger cells increased. This is exemplified by the boxplots' lengthening tails and increased incidence of outliers at higher passages. That trend resulted in a significantly larger median cell diameter and cell spread area of the population by passages 4 and 5, respectively, though many smaller cells still remained in the population. The larger adherent cells were not simply more spread, but in fact exhibited larger cell volumes, as confirmed by confocal images of BMSCs adhered to glass (Fig. S1A). Additionally, monitoring of suspended BMSCs as cells initially spread on and attach to a surface revealed that larger suspended cells did indeed produce larger adherent cells (Fig. S1B). Observations of BMSC size are typically stated in either the adherent or suspended state, so here we note the correlation in metrics of cell size in both states, and refer hereafter to the adherent cell spread area as "cell size."

However, from such images acquired at only a few selected time points, the cause of this apparent increase in average cell size is unclear. Static time points cannot distinguish between the sustained growth of individual cells and the changing ratios of subgroups each with inherently distinct cell sizes; both of these possibilities have been hypothesized previously (Wagner et al., 2010; Neuhuber et al., 2008). Do small cells become large over extended passaging? Alternatively, are larger and smaller cells two subpopulations with potentially distinct functionalities? The implications of the answers to these questions range from basic stem cell biology to strategies for stem cell-based therapies. Teasing out this distinction requires observation and tracking of individual cells over time in culture. We describe the procedure for and results from long-term imaging experiments designed to address these questions within a single passage, and then present a cell proliferation model designed to connect these results to observations across multiple passages.

Long-term imaging, tracking, and analysis

To better understand the increase in cell size over time in culture, we conducted long-term imaging experiments to monitor the growth of a population of BMSCs within a single passage. Cells at passage 5 were seeded on a fibronectin-coated glass plate and imaged every 10 min for 138 h (~6 days), starting 2 h after initial cell plating; see Materials and methods. A series of 10× images were taken in a 5 × 5 grid, in order to obtain a large enough field of view to encompass whole cell lineages (all of the descendants of a single cell) as cells divided and migrated, while still maintaining sufficient image resolution to track the cells. Figs. 2A–B shows the complete field of view at the beginning and end of imaging (see Video S1 for a movie of growth across all time points). Cells were tracked in a semi-automated manner and cell lineages constructed; see Materials and methods. In Figs. 2A–B, phase contrast images are overlaid with false color indicating the generation of each cell in relation to the start of the experiment (such that when a cell present in the original image divides, two "second generation" cells result and appear as a different color, and so on). Throughout the figures, these same colors are used to indicate each successive generation. Two such 5 × 5 grids were imaged at different locations on the same dish and, observing no large differences between locations, the results aggregated to increase the number of tracked cells. A complete repeat experiment was conducted with cells obtained from a different commercial source (i.e., a different cell donor). Results were qualitatively similar, and thus analogous graphs to those in the results below are shown in subplots of Supplemental Fig. S2 and referred to when appropriate. Figs. S2A–B show the complete field of view at the beginning and end of the repeat experiment.

Fig. 2C shows the number (and the population fraction, i.e., the fraction of the total number of cells present at that time; inset) of cells in each generation over time; see also Fig. S2C. After an initial lag period of approximately one

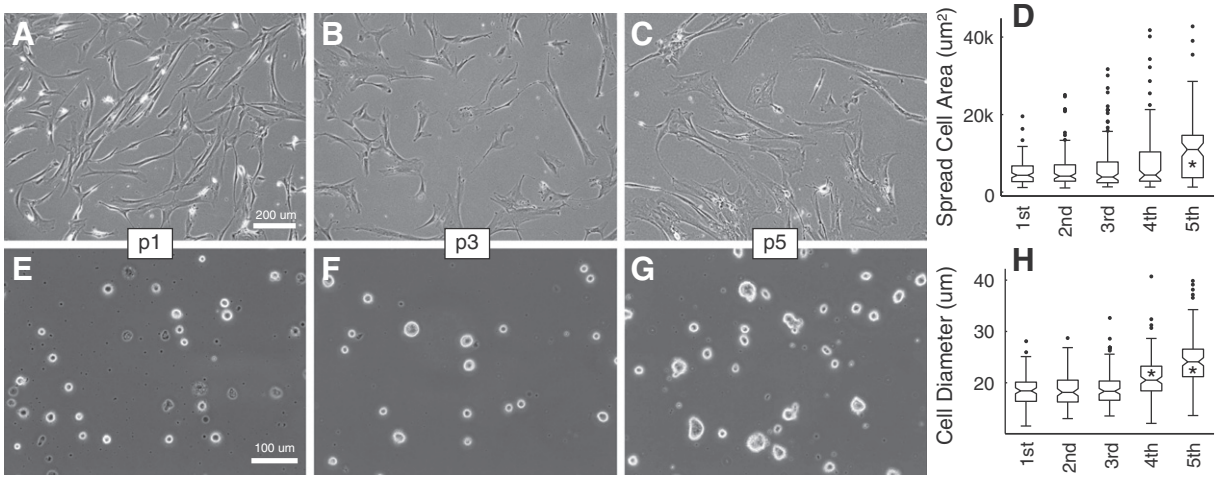

Figure 1 Adult human bone marrow stromal cell (BMSC) spread cell area and suspended cell diameter both increase over successive passages. (A–C) Phase contrast images of adherent BMSCs at the end of passages 1, 3, and 5. (D) Average spread cell area at the end of each of the first five passages. 100 cells were analyzed per passage. (E–G) Phase contrast images of suspended BMSCs at the end of passages 1, 3, and 5. (H) Average suspended cell diameter at the end of each of the first five passages. At least 91 cells were analyzed per passage. * indicates a median that is significantly different from all other passages at a $p < 0.05$ level.

day, some cells began to divide; the number of cells in each generation successively rose as cells of the previous generation divided, peaked, and declined as cells divided to produce daughter cells of the subsequent generation. Overall, from an original 190 cells and a surface coverage of 4%, the population expanded to 527 cells with a surface coverage of 18%. This represents ~1.5 total population doublings (2.8-fold expansion) and a doubling time of 3.9 days. However, within each generation, the lifetimes (time between cell divisions) of the cells that actually divided averaged between 0.9 and 1.4 days (Fig. 2D). The large discrepancy between the population average and that of individual cells arose because not all cells took part equally in the division process, consistent with previous models of stem cell proliferation (Deasy et al., 2003). This non-uniformity is apparent by the number of cells that remained in each generation without dividing (Fig. 2C) and the distribution of generations at ~6 days (Figs. 2A–B, color).

Fig. 2D shows cell lifetime as a function of cell size, for all cell divisions (excluding the first division in which the lifetime of cells is unknown). During the approximate hour

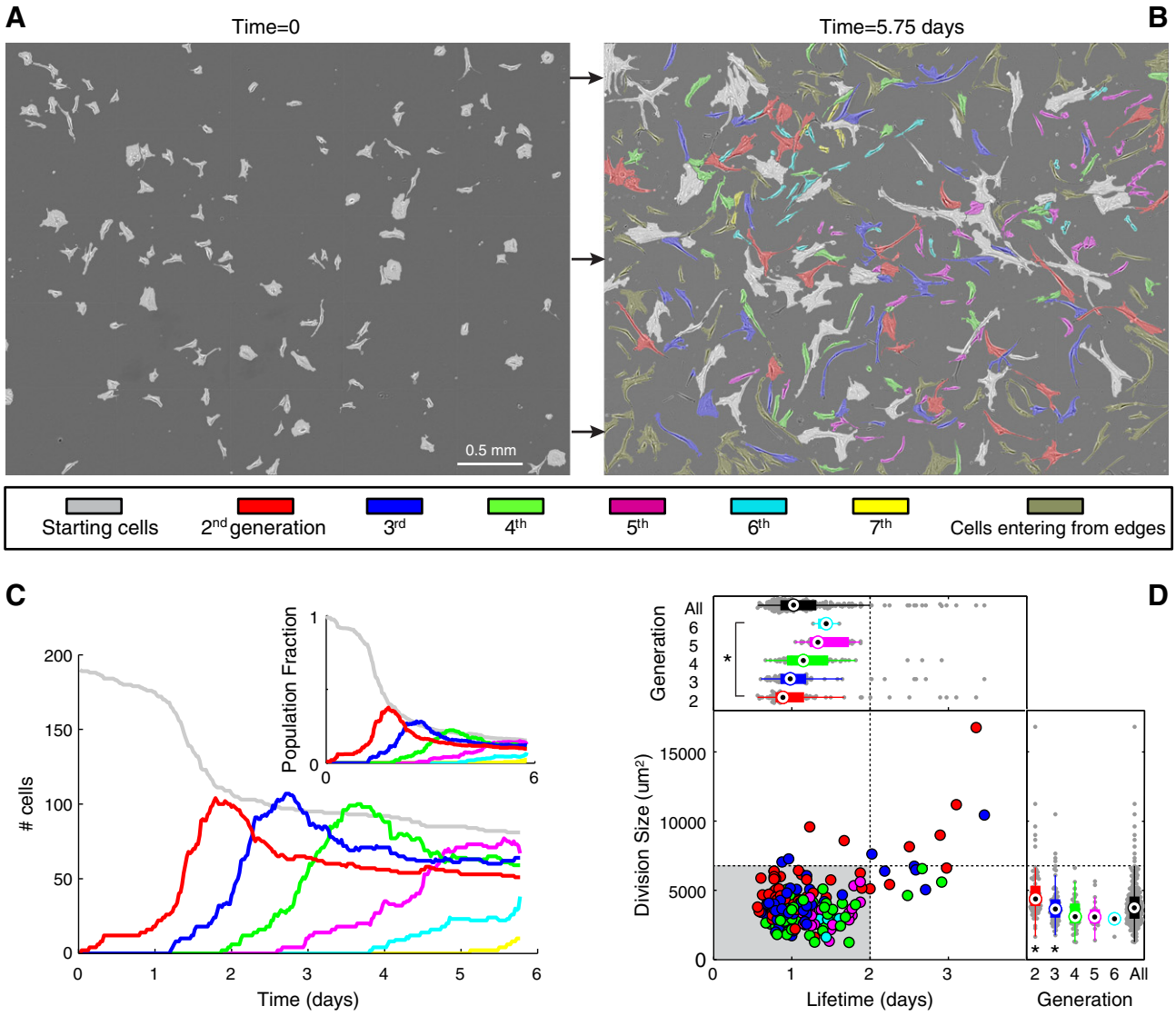

Figure 2 Overview of long-term cell tracking results for multiple generations of cells observed within a single passage (p5). (A–B) Phase contrast image of entire field of view at the beginning (A) and end (B) (5.75 days) of experiment with cells false colored to represent their generation as indicated in legend. All cells at time zero are classified as starting cells that produce two second-generation daughter cells upon division. (C) The number (and fraction of the total number of cells present at that time, inset) of cells in each generation over the course of the experiment shows the peak and decline of successive generations and also reveals that some cells stop dividing and remain in each generation. (D) The lifetime and size of cells at division reveal that 93% of cell divisions occur within 2 days with a size smaller than 7000 μm^2 (divisions of starting cells and cells entering the field of view are not included as their previous histories are unknown). The top (lifetime) and side (size) insets show the data from the overall population (black) and each generation individually as a beehive plot (gray circles) overlaid with a box and whisker plot. * indicates a statistically significant difference at a $p < 0.05$ level.

immediately prior to division, a cell rounds up before dividing to produce two smaller daughter cells that begin to grow and spread on the surface as they migrate away. To account for this, the division size is reported as the average of cell area over the time points 2–4 h prior to division. The top and side insets further detail the lifetime and size, respectively, for the overall population (black) and for cells in each generation (colors). Approximately 93% of cell divisions occurred within two days and for cell areas $<7000\ \mu m^2$; this range capturing the majority of cell division rates and sizes is indicated in the gray shaded region of Fig. 2D. As generation number increased, there was a trend toward longer lifetimes and smaller cell size prior to division (Fig. 2D top and side insets).

Division heterogeneity

Using these tracking data, individual cell lineages were constructed. Fig. 3A shows all daughter cells arising from one cell within the population over the duration of ~6 days. This lineage tree further indicates when the divisions occur (x-axis), the generation of each cell (color), and the relative spread cell area of each cell over time (line thickness). This graphical depiction of the lineage progression in vitro is qualitatively instructive: for example, daughter cells that did not divide over the observation period grew larger than those in the same generation that do divide. Moreover, comparing the lineages of the entire population provides a visually striking overview of the high degree of heterogeneity within

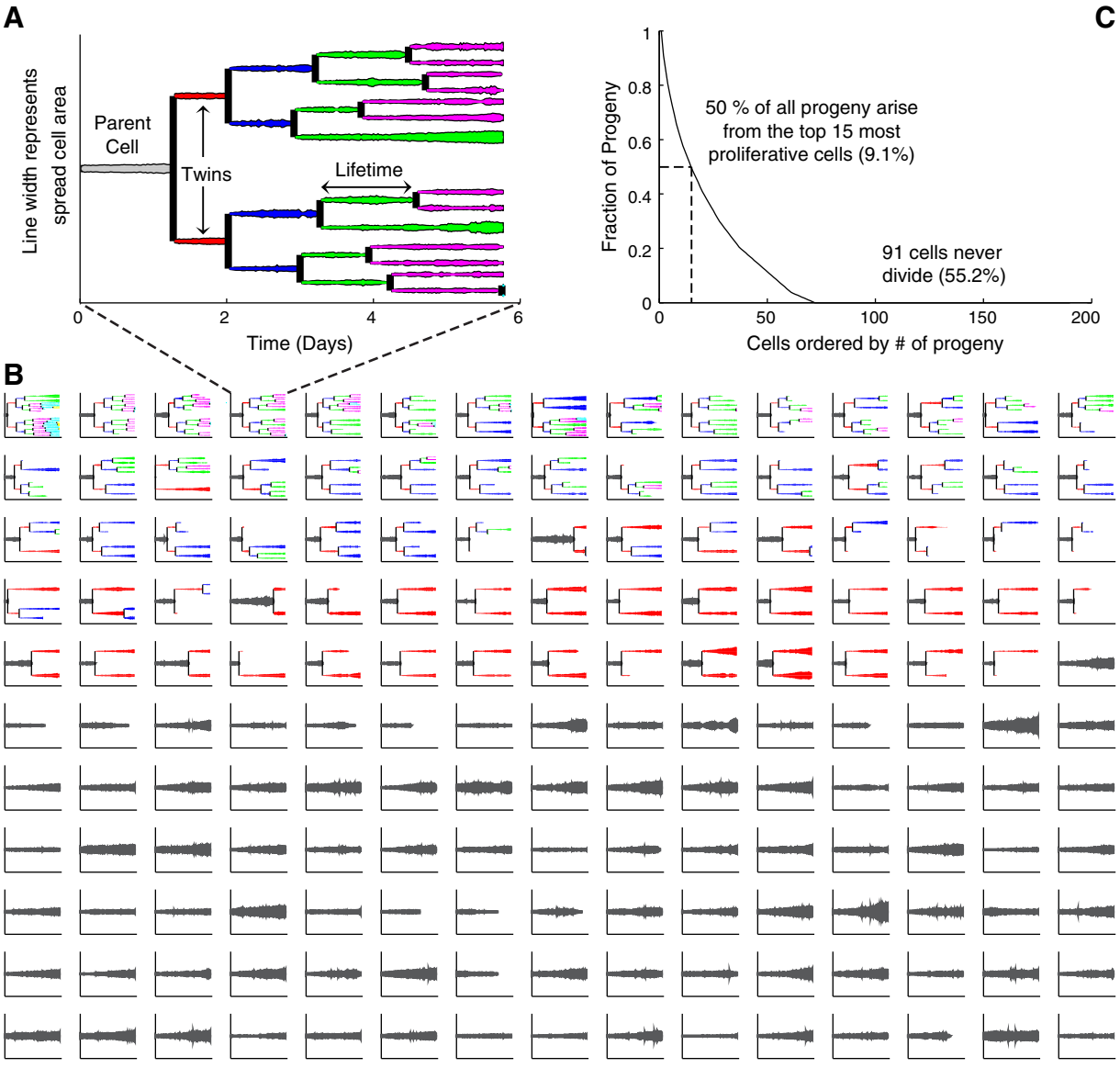

Figure 3 Heterogeneity in cell division within a single passage. (A) Example of lineage arising from a single cell. Line color represents generation and line width the spread cell area. (B) Lineages of starting cells ordered by the number of descendent cells (only those lineages wherein at least one cell stays within the field of view for at least three days shown). (C) Survival plot for the fraction of progeny remaining for cells ordered as in (B).

the population (Figs. 3B and S2D). Here, lineages were sorted in decreasing order of the total number of daughter cells arising from each original cell, and only those lineages for cells that remained within the field of view for at least 3 days are shown. Partial cell tracks are the result of a combination of cells migrating out of the field of view, detaching from the plate, or dying. Overall, 674 of the 800 cells comprising the lineages of the initial 190 cells remained until division or the end of the experiment (84.3%). Each daughter cell was considered a distinct entity such that parent cells ceased to exist upon division, and thus the total number of cells at the imaging conclusion was less than 800. A survival plot of the sorted lineages reveals that the 15 most proliferative cells (9.1%) accounted for over 50% of the increase in the cell number while 91 of the original cells (55.2%) never divided at all (Fig. 3C).

Quantifying increases in cell size over time

These data provide an answer to the question of how the differences in BMSC size arise under in vitro culture conditions. We found that the average spread area of BMSCs increased over time for cells within each generation (Figs. 4A and S2E). The rate of increase of ~3000 μm^2/day was consistent across generations, as shown in the Fig. 4A inset in which the time of emergence of each generation is offset to overlap. By setting a threshold of 7000 μm^2 for distinguishing between "larger" and "smaller" cells (see Fig. 2C), it is clear that the number and percentage of large cells increased over time (Figs. 4B and S2F, with large cells as dashed lines, small cells as dotted lines, and entire population of cells as solid lines). Only ten cells out of the 207 that reached this threshold ever divided (4.8%), while 219 of 246 cells that remained below this threshold divided within two days (89.0%). Fig. 4B can be separated into three regions. During the first day, few cells divided; cell spreading thus resulted in an increase in the fraction of large cells. In the following day, cell division dominated; this reduced the fraction of large cells but the not the number. For the remainder of the time, increases in the number of large cells outpaced cell division.

However, while the average size of cells within each generation increased, not all cells continued to grow larger. At the time of division, a cell rounds up, divides and produces two daughter cells that are initially smaller than the just-divided cell, but then begin to increase in area over time. Cell division in essence resets the cell size and growth trajectory. Thus, for dividing cells the spread area is maintained within a narrow range (as indicated by the sizes corresponding to cell division across generations in Fig. 2C). Cells that stopped dividing continue growing larger over time. This is illustrated in Fig. 4C, which compares growth in

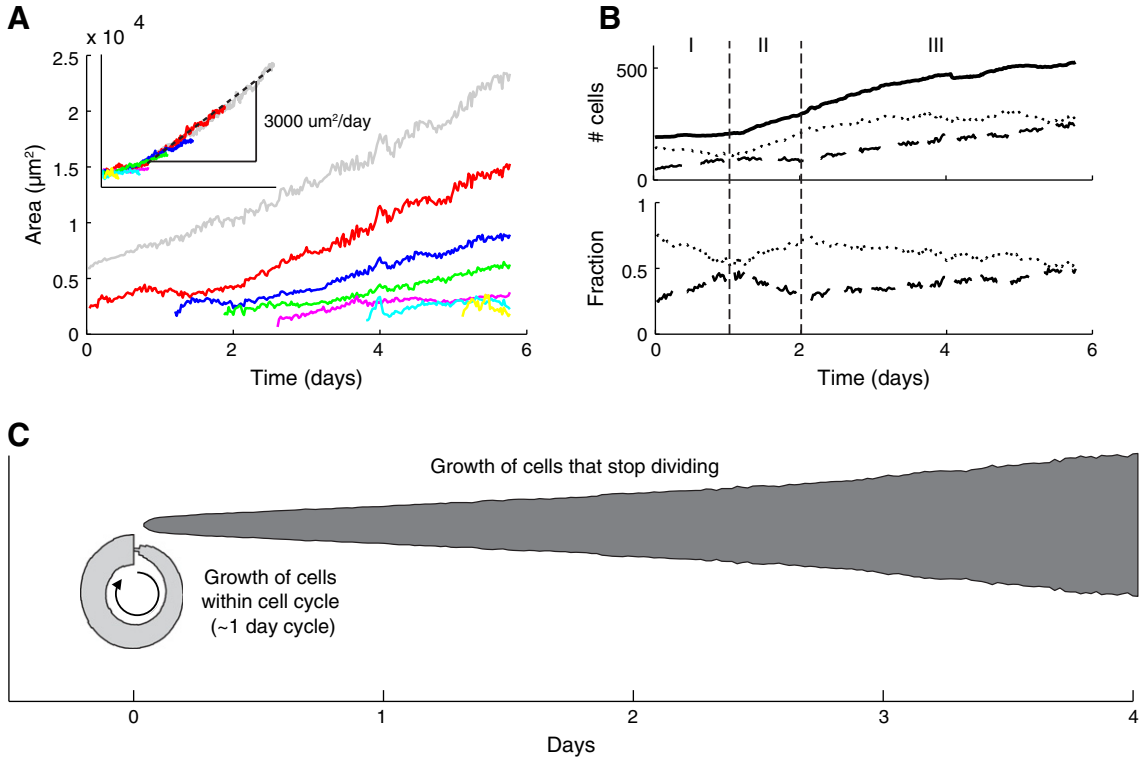

Figure 4 Increase in spread cell area over time. (A) The average cell area for BMSCs of each generation increases. Inset: offsetting each successive generation so that they overlap shows a conserved linear size increase of ~3000 μm^2/day. (B) The number and fraction of small (dotted line) and large (dashed line and defined as those cells with area above the 7000 μm^2 threshold shown in Fig. 2D) cells, along with the overall number of cells (solid line), over time. This indicates three regimes: I. cell spreading with few divisions; II. cell division dominates; and III. size growth outpaces cell divisions. (C) Area growth for cells within the cell cycle (light gray) compared to growth of cells that have stopped dividing (dark gray). Line width represents average spread cell area.

cell area for cells that divided to those that did not. Note that this figure appears as a schematic, as we did not intend to pinpoint the stage of the cell cycle exit, but that the width of the regions corresponding to cell size is taken from the actual timelapse data. Cells that remained within the cell cycle grew cyclically larger up to the point of division; those that did not divide within two days grew much larger. This analysis thus discriminated increased cell size due to progression through the cell cycle from the comparatively larger increase in area of those cells that did not divide. These data provide a clear picture of the emergence of larger cells that has previously only been observed at a population level. Note that this analysis is of multiple generations within a single passage; we revisit consideration of multiple passages in the section, Modeling cell population changes across passages in culture.

Reasons for heterogeneity: Intrinsic vs. extrinsic factors

In addition to the large degree of heterogeneity observed across the whole population, as demonstrated in Fig. 3, non-uniform cell division occurred within individual lineages. Was this due primarily to intrinsic factors, or to extrinsic factors such as cell–cell contact? To investigate the extent and potential causes for the heterogeneity, we grouped the two daughter cells formed from each cell division (here termed "twins" for simplicity) by the corresponding replication behavior. As shown in Fig. 5A, we identified sets of twins in which both daughter cells subsequently divided (green), one daughter cell divided (yellow) while its twin did not (orange) – here, termed asymmetric cell division fate – or neither cell divided (red). A cutoff of two days was used to classify a cell as non-dividing, as 93.5% of observed divisions occurred within this time frame (see Fig. 2C). Pairs that could not be classified, either due to the elimination of a cell from the field of view or the end of the experiment, were excluded from this analysis. Using these metrics of twin classification, we identified 78 pairs of twins in which both daughter cells subsequently divided, 28 pairs in which only a single daughter cell divided, and 59 pairs in which neither daughter cell divided.

We then considered factors that could influence cell division decisions. Perhaps individual cells received physical cues from the surroundings, such as cell contacts that were influencing the division process (extrinsic factors). Alternatively (or additionally), cell fate could be determined at the time of division depending more on the parent cell and lineage history (intrinsic factors). To obtain insights into this distinction, we quantified the average number and extent of cell–cell contacts at each time point and cumulatively over time, as well as the average past presence of cells along the migration path of each cell (Fig. 5B). Extent of cell contacts was reported as the percentage of cell periphery in contact with other cells. Cells also secrete and modify the surrounding extracellular matrix proteins, which could in turn generate new structural, mechanical, or biochemical cues for other cells that subsequently migrate along the deposited extracellular matrix proteins (Ingber and Folkman, 1989). Details of this metric's calculation can be found in Fig. S2. To quantify each of these metrics for cells that did not divide, average values were acquired for the time corresponding to the lifetime of its twin (in the case of asymmetric cell division fate) and for the average lifetime of dividing cells (when neither twin divided). To consider potential intrinsic, lineage-related differences, we also quantified the size and lifetime of each of the three twin categories, the corresponding parent cells, and the corresponding "grandparent" cells (Fig. 5C, where again lineage width indicates cell size). The insets in Fig. 5C show these averages individually for each of the twin categories, and these data are overlaid in the annotated graphic beside the insets.

No significant differences were identified between our twin groupings using the extrinsic factors of mean number of cell–cell contacts, mean percent of the cell in contact with other cells, cumulative number of cell–cell contacts, and the previous presence of cells (Fig. 5B). There was thus no evidence that these physical cues strongly affected whether a cell divided or not. In fact, anecdotally, cells with the most cell–cell contact that migrated alongside, or even directly over other cells, were often part of the lineages that were the most actively dividing. We also considered that the timing of the physical cues could have an effect that would not be identified when considering only the average over the lifetime of the cell, but this type of time sensitive analysis also indicated no significant differences (Figs. S3, S4). Migration velocity varied widely for a given cell over cell lifetime, and no significant differences were identified to suggest correlations with migration velocity and cell cycle exit (data not shown); other migration parameters were not considered.

In contrast, with this capacity to look back in time at the lineage of cells that stopped dividing, we found that apparent differences already existed in the parent cells that gave rise to the different twin categories. Fig. 5C shows that the average parent cell lifetime of twins that both divided (green) was significantly shorter than the lifetime of parents of cells that both stopped dividing (red). The parent lifetime for twins with asymmetric cell division fate was in between these two values. Cells that had stopped dividing grew in size at a faster rate than dividing cells, although this trend was not observed for the parent cells. No significant differences were observed in the size or growth rate of grandparents of these twin categories, though we note that these data are sparser due to the experiment timescale. Our results provide indications that immediate cell division decisions were influenced more by the intrinsic factors of the cell than the immediate extrinsic factors that were considered.

To obtain a better understanding of the larger cells that stop dividing, we stained BMSCs grown under similar conditions for senescence-associated β-galactosidase. After a week of growth, nearly all of the larger cells stained positively for this marker of replicative senescence that increases with cumulative population doublings and age (Dimri et al., 1995), while most smaller cells did not (Fig. 5D). This finding indicates that the large cells are not simply quiescent but are senescent. The cell cycle position of these cells was not determined conclusively in the attached state (and analysis in the suspended state would have compared only population averages); however, it is generally understood that the cell cycle arrests in the transition from phase G1 to S (Sherwood et al., 1988). It is established in several other cell types that

replicative senescence can be concomitant with sustained metabolic activity (Goldstein, 1990). Although it is beyond the scope of the current investigation, future studies could be designed to ascertain whether these larger cells are also committed progenitors of one or more mesenchymal lineages. Note that for such studies to indicate findings stronger than correlative comparisons among populations, live-cell indicators of commitment would be advantageous.

Modeling cell population changes across passages in culture

Finally, we considered how our observations within a single passage related to the changes in cell size across several passages, as shown in Fig. 1 to illustrate the anecdotal observation that median cell size of the population tends to increase with increasing passage number. We thus developed a simplistic model for cell division, senescence, and size growth (see Supplemental). We first validated that the model was capable of reproducing our within-passage observations. Fig. 6A shows that this model quantitatively produced the characteristic rise, peak, and fall of subsequent generations (reported experimentally in Fig. 2B), as well as the increase in cell spread area for cells within each generation (reported experimentally in Fig. 4A). For these simulations, the starting number (190) and senescent fraction (0.34) of cells and the probability of cell division (based on a gamma distribution) were set from our experiments, with the senescence probability k_s as the only

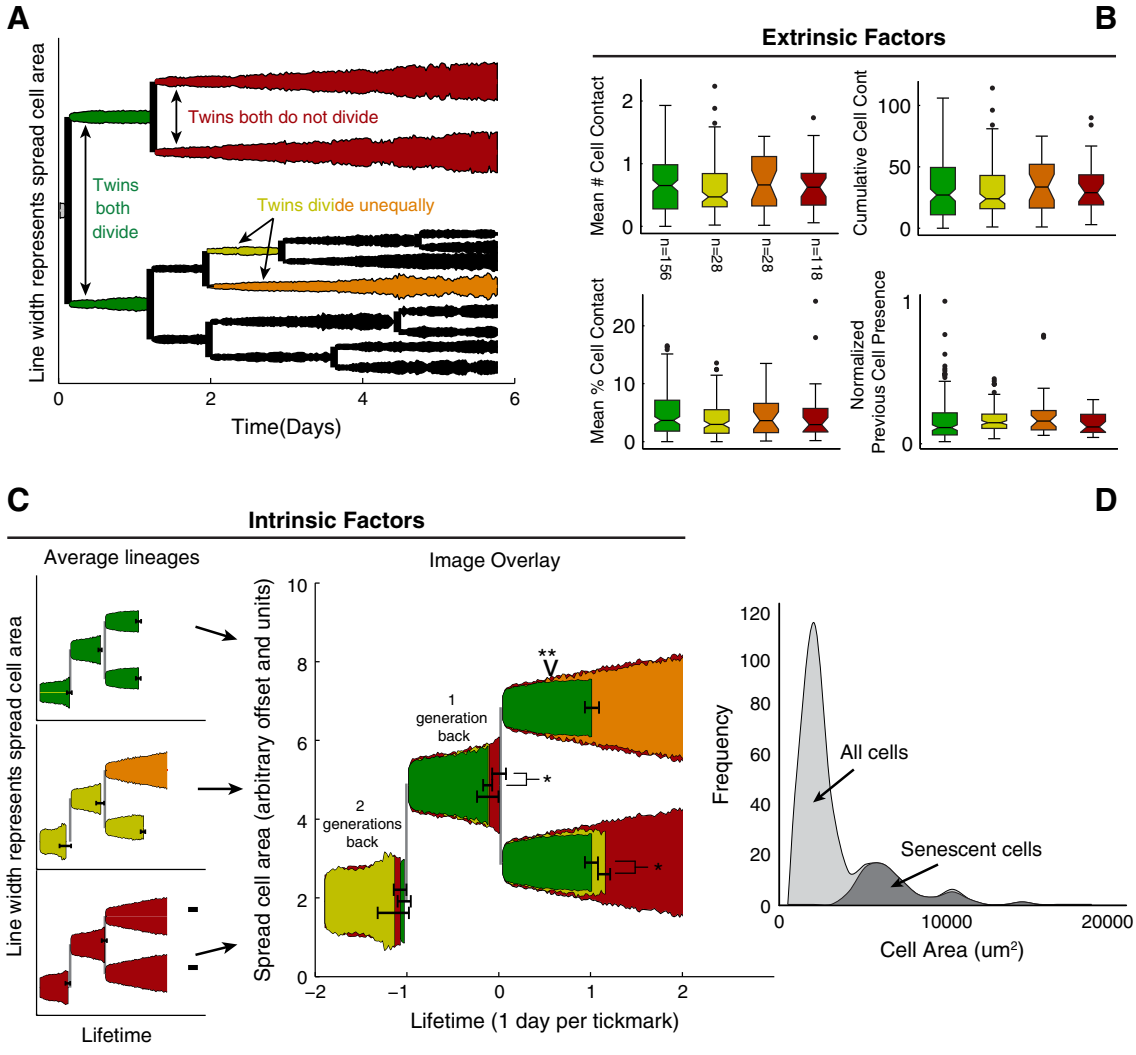

Figure 5 Considering potential reasons for size heterogeneity among BMSCs. (A) Cell lineage with heterogeneous divisions with cases with twins that both divide (green), one divides (yellow) and one does not (orange), or both do not divide (red). (B) Extrinsic factors that could potentially influence cell division decisions. Contact defined as another cell within 12.9 μm. No significant differences seen for any of these factors. (C) The average lineage history of the cells (intrinsic factors) for each of the three groups overlaid and individually (inset). Line width represents spread cell area. Error bars indicate 95% confidence intervals for lifetime. * denotes significance at a $p < 0.05$ level and ** marks the time that the cell area for dividing and non-dividing cells becomes significantly different ($p < 0.05$). (D) Large cells are predominately senescent. The overall distribution of cell sizes and those that stained positive for the cell senescence indicator β-galactosidase after 7 days of in vitro culture.

fitting parameter. To then extend this analysis to multiple passages, Fig. 6B shows that we estimated the population fraction of senescent cells at the end of each passage for BMSCs in culture, by reanalyzing the experimental data from adherent cells (Fig. 1) using a range of size cutoffs centered around the senescence cutoff identified in our experiments (7000 ± 1500 μm^2). We then applied the cell lifetime and senescence probability identified in Fig. 6B to an initial simulated population (generation 1) of 25 cells for 33 days of growth equivalent to passage 2 through 5. Fig. 6C (top) shows the experimental data (black points) as compared to model predictions for these assumptions of fixed, passage-independent cell lifetime and senescence probability (lines). For several such passage-independent parameter combinations, this model did not reproduce the experimentally observed increase in the fraction of large (senescent) cells over weeks in vitro. In fact, no set of fixed parameters was able to recreate the observed increase, with the senescent fraction reaching a plateau determined by the ratio of lifetime and senescent probability. Instead, either an increasing senescence probability over time (Fig. 6C, middle) or an increasing cell lifetime (Fig. 6C, bottom), while maintaining other parameters fixed, could explain the increase in mean cell size with increasing passaging. Note that the time dependence of the senescence probability and cell lifetime was varied iteratively to obtain a reasonable fit to the experimental data, given this stochastic simulation model. While we do not intend to draw definitive conclusions as to the exact rates or time dependence of these rates from such a simple model, these results do suggest that at least one of these rates must change over time in culture to explain the anecdotally and experimentally observed increase in large and senescent cells upon in vitro expansion of BMSCs.

Discussion

Through timelapse imaging and analysis of BMSC division and morphology, we observed both known and unanticipated changes in cell size over time. It is well established that cell size increases as a eukaryotic cell replicates genetic material while traversing through the normal cell replication cycle (Cooper, 2000), and that this cyclic increase in cell volume also occurs for putative BMSCs in vitro (Lee et al., 2011). However, we observed directly that an appreciable fraction of BMSCs did not replicate over ~6 days in vitro (55.2%), and that most of the resulting progeny could be traced back to only 9% of the cells attached at day 1. The heterogeneity in both cell proliferation and lineage tree types (Fig. 3B) is not wholly unexpected, but is nonetheless striking. Note that one consequence of this low fraction of faster-replicators within a larger population of slower- (or non-) replicators means that a reported population doubling

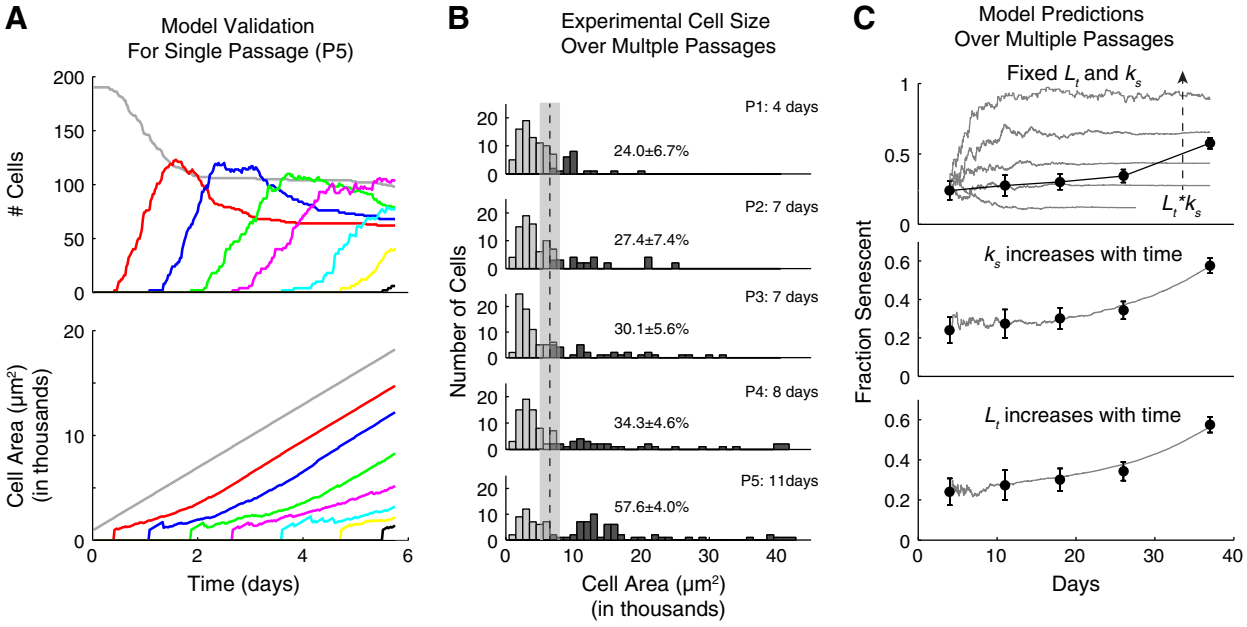

Figure 6 Model to provide insight into the changing cell population across multiple passages. (A) Both generational cell division peaks (see Fig. 2C) and cell size growth rates (see Fig. 4A) can be reproduced by this model, with senescence probability as the only adjustable parameter not taken from experiments. (B) Experimentally derived distribution of cell spread area (from same cell expansion as Fig. 1) for each passage up to p5 overlaid with a cutoff (dashed line, 7000 ± 1500 μm) to distinguish small replicating cells from the larger putatively senescent cells. The length of each passage and fraction of senescent cells determined by this size cutoff were used for model predictions over multiple passages in (C). The percentage of senescent cells within each passage is indicated. (C) Based upon the model validated within a single passage in (A), no fixed magnitude of senescence probability (k_s) and cell lifetime (L_t) (gray lines) can reproduce the experimentally measured fraction of senescent cells (black circles, mean ± standard deviation) over several passages in culture (top). However, increasing the assumed senescence probability (middle) or increasing the cell lifetime (bottom) over time can each reproduce these trends.

time poorly represents the number of times that individual, replicating BMSCs have divided. This distinction may be consequential for future studies of single cell profiling and therapeutic applications that require culture expansion of BMSCs and identification of bone marrow-derived mesenchymal stem cells with ostensibly low population doublings.

Further, through these growth rate-tagged lineages, we concluded that smaller cells within the BMSC population were not a distinct subpopulation that existed at day 1, proliferating with a distinct doubling time and maintaining a distinct and smaller cell size. Likewise, the larger cells within that population were not a distinct and persistent lineage. Instead, we found that smaller cells became larger cells as those cells exited the cell cycle. In fact, larger cells not only grew and failed to divide within the observed 2 days typical of 93% of the actively dividing population, but larger cells also showed a biochemical marker of senescence. We observed no indication over this limited timescale, or over the five passages summarized in Figs. 1 and 6B, that the smaller cells replicated to such an extent that this subpopulation remained small but reached a Hayflick limit (Hayflick and Moorhead, 1961). We note that the larger cells were those that had divided the least, but that we cannot report the full history of the larger cells that were seeded on day 1.

We further note, as highlighted in our introduction, that initial heterogeneity of cell size and/or behavior within an in vitro culture of BMSCs can be attributed to several factors not considered explicitly here. These include ex vivo reprogramming (Zipori, 2010), genetic mutations (Wagner et al., 2010), differences among cells in commitment maturity (Ratajczak et al., 2008) toward a particular differentiation endpoint that can manifest as a wide distribution of metabolic expression profiles (McMurray et al., 2011), differences in cell cycle stages (Lee et al., 2011), and variation in culture conditions among many cells in a single tissue-culture dish (Bruder et al., 1997). Thus, understanding of how and when morphologically distinct cells within the in vitro BMSC population relate via cell division lineages, particularly under conditions of culture expansion that are intended to replicate that population for in vitro and in vivo applications, is of practical and scientific interest.

We replicated this imaging study at two locations within the same culture vessel, as well as in a separate timelapse experiment with cells obtained from a different commercially purified source and grown following a different cell seeding density protocol. The general trends of increasing cell size within each generation and heterogeneity across the population were observed consistently. However, not surprisingly, the exact thresholds for cell lifetime and cell size beyond which replication and senescence change markedly can differ among cell sources and culture conditions.

Thus, with these data we assert that small replicating cells do not "become" large replicating cells upon culture expansion of BMSCs. Nor are those large cells "old", in the sense that these cells are from earlier generations that gradually increase in cell size with time in vitro. Rather, large cells within an MSC subculture are chiefly those cells that failed to divide within the typical cell lifetime. This statement is consistent with some observations of replicative senescence in BMSCs (Wagner et al., 2008) and other cell types (e.g., fibroblasts that reach growth arrest are often described as uncharacteristically large or as increasingly spindly (Bayreuther et al., 1988)). Notwithstanding this retrospective similarity, the origin and onset of larger cells within putative BMSC cultures have been much less clear, owing to the comparatively larger degree of heterogeneity in cell sources, cell purification methods, and reported metrics of both morphology and biological behaviors. Building on such observations based on a single passage, our model shows that increased mean cell size of the population over multiple passages can be predicted by increases in either (or both) the cell senescence probability or lifetime of individual cells with increased passaging.

Under all conditions and imaging durations considered, the cells were subconfluent; yet, the fraction of larger cells increased steadily. This may strike one as in contrast to the notion often discussed that BMSCs become larger (over multiple passages) when cultured at higher cell densities. In fact, Prockop et al. noted that BMSCs should be passaged at ~70% confluency to maintain an appreciable fraction of the smaller, rapidly proliferating and spindly cells (Wolfe et al., 2008). Although we do not disagree with that recommendation, we find no evidence in the present study that either cell–cell or cell–matrix contact strongly modulates whether a cell exits the cell cycle and then becomes significantly larger. Instead, the comparison of parent cells of twin daughter cells that either both replicated or both failed to replicate (Fig. 5C) indicated that intrinsic factors play at least an early role in this cell fate decision. Larger parent cells beget larger daughter cells, and twins are more likely to behave similarly than differently. From the present study, we do not resolve whether extrinsic factors contribute a further, downstream effect on division rate, senescence probability, or lineage commitment. Although we aimed to be thorough in our consideration of physical cues such as the number and extent of cell–cell contact and interactions with areas previously occupied by cells under the assumption of standard in vitro culture expansion conditions, we cannot rule out the possibility that these or other physical cues (or intrinsic differences in protein expression) could also play an early role. For example, the image resolution and analysis method restricted our definition of cell–cell contact to cells within 12.9 μm of each other, and could thus overestimate contact in cases where cells approach within this range but do not truly contact. Sensitivity analysis ranging the contact threshold from 12.9 μm to 25.8 μm did not reveal any new or strong correlations with cell area (data not shown). This lack of correlation does not obviate contact-mediated modulation of cell fate, but suggests that the transition from replicating to senescent and larger BMSCs is not wholly determined by contact when cells are subconfluent.

To minimize disruption of cell behavior from typical in vitro conditions during timelapsed observations, no in situ or live staining of the cells was conducted. Thus, real-time, single-cell correlations between the cell morphology and division rate with the cell cycle, senescence, differentiation, or other markers were not included. As the present experiments were conducted under otherwise standard in vitro culture expansion conditions, one can reasonably apply observations from related in vitro experiments at a fixed timepoint, such as β-gal evaluation of senescence as a function of cell size at that timepoint. Real-time correlations present intriguing opportunities for further study, and can benefit from the semi-automated image analysis reported herein. Additionally, although the stochastic model employed

showed that the observed trend of increasing average cell size with increasing passage number requires that either the senescence probability or the cell division rate changes with passage number, more sophisticated models such as those developed by Krinner et al. (2010) could incorporate these observations and identify the more influential factor. Our model and experiments included identification of a cell size and cell lifetime beyond which senescence was statistically likely. We note that variables – such as the patient or tissue cell source, harvesting and isolation procedures, media and sera lots, seeding density, and passaging techniques, among others – can influence the senescence probability and division rate significantly. However, the main findings appear robust to many of these variables.

In summary, direct observation of human BMSC division indicates that within a given passage, larger cells are neither a distinct, replicating subpopulation nor solely an older subpopulation that has become larger with increased in vitro passaging. Instead, the larger cells represent a collection of cells from many different generations that have ceased to self-replicate in vitro; the capacity for self-renewal in vitro has been considered part of the definition of mesenchymal stem cells, and thus the larger cells do not fulfill this criterion. Contrastingly, the smaller cells are mitotically active. Though beyond the scope of this study, efforts are underway to elucidate further differences among these cells through continuous size-based sorting (Lee et al., 2011). This understanding of the onset of heterogeneity within culture-expanded BMSCs, as well as the image analysis and modeling that enabled data interpretation, can help guide future studies that aim to isolate, study, or deploy mesenchymal stem cells for predictable outcomes.

Acknowledgments

We thank R. Jolibois-Quinot, S. Bandara, and L.M. Nyan for their assistance with image analysis, and S. Hui for confocal image acquisition. We gratefully acknowledge funding from the National Research Foundation of Singapore through the Singapore–MIT Alliance for Research and Technology (SMART)'s BioSystems and Micromechanics (BioSyM) Interdisciplinary Research group.

Appendix A. Supplementary data

Supplementary data to this article can be found online at http://dx.doi.org/10.1016/j.scr.2013.09.004.

References

Bayreuther, K., et al., 1988. Human skin fibroblasts in vitro differentiate along a terminal cell lineage. Proc. Natl. Acad. Sci. 85 (14), 5112–5116.

Bianco, P., Robey, P.G., Simmons, P.J., 2008. Mesenchymal stem cells: revisiting history, concepts, and assays. Cell Stem Cell 2 (4), 313–319.

Bruder, S.P., Jaiswal, N., Haynesworth, S.E., 1997. Growth kinetics, self-renewal, and the osteogenic potential of purified human mesenchymal stem cells during extensive subcultivation and following cryopreservation. J. Cell. Biochem. 64 (2), 278–294.

Caplan, A.I., 1991. Mesenchymal stem cells. J. Orthop. Res. 9 (5), 641–650.

Carpenter, A.E., et al., 2006. Cell profiler: image analysis software for identifying and quantifying cell phenotypes. Genome Biol. 7 (10), R100.

Colter, D.C., et al., 2000. Rapid expansion of recycling stem cells in cultures of plastic-adherent cells from human bone marrow. Proc. Natl. Acad. Sci. U. S. A. 97 (7), 3213–3218.

Colter, D.C., Sekiya, I., Prockop, D.J., 2001. Identification of a subpopulation of rapidly self-renewing and multipotential adult stem cells in colonies of human marrow stromal cells. Proc. Natl. Acad. Sci. U. S. A. 98 (14), 7841–7845.

Cooper, G., 2000. The Cell: A Molecular Approach. Sinauer Associates, Sunderland (MA).

Costa, M.R., et al., 2011. Continuous live imaging of adult neural stem cell division and lineage progression in vitro. Development 138 (6), 1057–1068.

Darling, E.M., et al., 2008. Viscoelastic properties of human mesenchymally-derived stem cells and primary osteoblasts, chondrocytes, and adipocytes. J. Biomech. 41 (2), 454–464.

Deasy, B., et al., 2003. Modeling stem cell population growth: incorporating terms for proliferative heterogeneity. Stem Cells 21 (5), 536–545.

Dimri, G.P., et al., 1995. A biomarker that identifies senescent human cells in culture and in aging skin in vivo. Proc. Natl. Acad. Sci. 92 (20), 9363–9367.

Dominici, M., et al., 2006. Minimal criteria for defining multipotent mesenchymal stromal cells. The International Society for Cellular Therapy position statement. Cytotherapy 8 (4), 315–317.

Eilken, H.M., Nishikawa, S.-I., Schroeder, T., 2009. Continuous single-cell imaging of blood generation from haemogenic endothelium. Nature 457 (7231), 896–900.

Goldstein, S., 1990. Replicative senescence: the human fibroblast comes of age. Science 249 (4973), 1129–1133.

Haack-Sørensen, M., et al., 2012. Mesenchymal stromal cell phenotype is not influenced by confluence during culture expansion. Stem Cell Rev. Rep. 1–15.

Halfon, S., et al., 2010. Markers distinguishing mesenchymal stem cells from fibroblasts are downregulated with passaging. Stem Cells Dev. 20 (1), 53–66.

Hare, J.M., et al., 2012. Comparison of allogeneic vs. autologous bone marrow-derived mesenchymal stem cells delivered by transendocardial injection in patients with ischemic cardiomyopathy: the POSEIDON randomized trial mesenchymal stem cells and ischemic cardiomyopathy. JAMA 308 (22), 2369–2379.

Hayflick, L., Moorhead, P.S., 1961. The serial cultivation of human diploid cell strains. Exp. Cell Res. 25 (3), 585–621.

Ingber, D.E., Folkman, J., 1989. Mechanochemical switching between growth and differentiation during fibroblast growth factor-stimulated angiogenesis in vitro: role of extracellular matrix. J. Cell Biol. 109 (1), 317–330.

Knoepfler, P.S., 2009. Deconstructing stem cell tumorigenicity: a roadmap to safe regenerative medicine. Stem Cells 27 (5), 1050–1056.

Krinner, A., et al., 2010. Individual fates of mesenchymal stem cells in vitro. BMC Syst. Biol. 4 (1), 73.

Kuznetsov, S.A., et al., 1997. Single-colony derived strains of human marrow stromal fibroblasts form bone after transplantation in vivo. J. Bone Miner. Res. 12 (9), 1335–1347.

Lee, W.C., et al., 2011. High-throughput cell cycle synchronization using inertial forces in spiral microchannels. Lab Chip 11 (7), 1359–1367.

Maloney, J.M., et al., 2010. Mesenchymal stem cell mechanics from the attached to the suspended state. Biophys. J. 99 (8), 2479–2487.

McMurray, R.J., et al., 2011. Nanoscale surfaces for the long-term maintenance of mesenchymal stem cell phenotype and multipotency. Nat. Mater. 10 (8), 637–644.

Muraglia, A., Cancedda, R., Quarto, R., 2000. Clonal mesenchymal progenitors from human bone marrow differentiate in vitro according to a hierarchical model. J. Cell Sci. 113 (Pt 7), 1161–1166.

Neuhuber, B., et al., 2008. Effects of plating density and culture time on bone marrow stromal cell characteristics. Exp. Hematol. 36 (9), 1176–1185.

Oswald, J., et al., 2004. Mesenchymal stem cells can be differentiated into endothelial cells in vitro. Stem Cells 22 (3), 377–384.

Pevsner-Fischer, M., Levin, S., Zipori, D., 2011. The origins of mesenchymal stromal cell heterogeneity. Stem Cell Rev. Rep. 7 (3), 560–568.

Ratajczak, M.Z., et al., 2008. Bone marrow—home of versatile stem cells. Transfus. Med. Hemother. 35 (3), 248–259.

Ravin, R., et al., 2008. Potency and fate specification in CNS stem cell populations in vitro. Cell Stem Cell 3 (6), 670–680.

Scherf, N., et al., 2012. On the symmetry of siblings: automated single-cell tracking to quantify the behavior of hematopoietic stem cells in a biomimetic setup. Exp. Hematol. 40 (2), 119–130 (e9).

Schroeder, T., 2011. Long-term single-cell imaging of mammalian stem cells. Nat. Methods 8 (4 s), S30–S35.

Seeger, F.H., et al., 2007. Cell isolation procedures matter: a comparison of different isolation protocols of bone marrow mononuclear cells used for cell therapy in patients with acute myocardial infarction. Eur. Heart J. 28 (6), 766–772.

Sherwood, S.W., et al., 1988. Defining cellular senescence in IMR-90 cells: a flow cytometric analysis. Proc. Natl. Acad. Sci. 85 (23), 9086–9090.

Siddappa, R., et al., 2007. Donor variation and loss of multipotency during in vitro expansion of human mesenchymal stem cells for bone tissue engineering. J. Orthop. Res. 25 (8), 1029–1041.

Treiser, M.D., et al., 2010. Cytoskeleton-based forecasting of stem cell lineage fates. Proc. Natl. Acad. Sci. 107 (2), 610–615.

von Bahr, L., et al., 2012. Long-term complications, immunologic effects, and role of passage for outcome in mesenchymal stromal cell therapy. Biol. Blood Marrow Transplant. 18 (4), 557–564.

Wagner, W., et al., 2008. Replicative senescence of mesenchymal stem cells: a continuous and organized process. PLoS One 3 (5), e2213.

Wagner, W., Ho, A.D., Zenke, M., 2010. Different facets of aging in human mesenchymal stem cells. Tissue Eng. B Rev. 16 (4), 445–453.

Wolfe, M., et al., 2008. Isolation and culture of bone marrow-derived human multipotent stromal cells (hMSCs). Mesenchymal Stem Cells. Springer, pp. 3–25.

Xu, W., et al., 2004. Mesenchymal stem cells from adult human bone marrow differentiate into a cardiomyocyte phenotype in vitro. Exp. Biol. Med. (Maywood) 229 (7), 623–631.

Ylostalo, J., Bazhanov, N., Prockop, D.J., 2008. Reversible commitment to differentiation by human multipotent stromal cells in single-cell-derived colonies. Exp. Hematol. 36 (10), 1390–1402.

Zipori, D., 2010. The hemopoietic stem cell niche versus the microenvironment of the multiple myeloma-tumor initiating cell. Cancer Microenviron. 3 (1), 15–28.

Zomorodian, E., Baghaban Eslaminejad, M., 2012. Mesenchymal stem cells as a potent cell source for bone regeneration. Stem Cells Int. 2012.